Copyright ⓒ 2023 KSII

An ANN-based Intelligent Spectrum Sensing Algorithm for Space-based Satellite Networks

Xiujian Yang[1], and Lina Wang[1*]
[1] School of Computer and Communication Engineering, University of Science and Technology Beijing
Beijing, 100083 China
[e-mail: xj995995@163.com, wln_ustb@126.com]
[*]Corresponding author: Lina Wang

Received December 3, 2022; revised January 20, 2023; accepted March 3, 2023; published March 31, 2023

Abstract

In Low Earth Orbit (LEO) satellite networks, satellites operate fast and the inter-satellite link change period is short. In order to sense the spectrum state in LEO satellite networks in real-time, a space-based satellite network intelligent spectrum sensing algorithm based on artificial neural network (ANN) is proposed, while Geosynchronous Earth Orbit (GEO) satellites are introduced to make fast and effective judgments on the spectrum state of LEO satellites by using their stronger arithmetic power. Firstly, the visibility constraints between LEO satellites and GEO satellites are analyzed to derive the inter-satellite link building matrix and complete the inter-satellite link situational awareness. Secondly, an ANN-based energy detection (ANN-ED) algorithm is proposed based on the traditional energy detection algorithm and artificial neural network. The ANN module is used to determine the spectrum state and optimize the traditional energy detection algorithm. GEO satellites are used to fuse the information sensed by LEO satellites and then give the spectrum decision, thereby realizing the inter-satellite spectrum state sensing. Finally, the sensing quality is evaluated by the analysis of sensing delay and sensing energy consumption. The simulation results show that our proposed algorithm has lower complexity, the sensing delay and sensing energy consumption compared with the traditional energy detection method.

Keywords: Low Earth Orbit (LEO), inter-satellite links, intelligent sensing, spectrum state, artificial neural networks (ANN)

This paper is supported by the National Natural Science Foundation of China under Grants No. 61701020.

http://doi.org/10.3837/tiis.2023.03.016 **ISSN : 1976-7277**

1. Introduction

The deployment of 5G mobile systems has already started at the end of October 2019, and academia and industry have begun to conceptualize the direction and basic specifications for the next generation of mobile systems (6G). Driven by the exponential growth of data traffic and the continuous demand for three-dimensional ubiquitous access in the whole area, 6G systems need to integrate communication with computing, intelligence, and sensing technologies to build an integrated network that can support large-scale wireless connectivity, realizing a 6G era in which everything is intelligently connected and the digital and physical worlds are deeply integrated [1].

The 6G network will form a three-dimensional mobile communication network through GEO satellite networks, medium- and LEO satellite networks, airborne networks, and terrestrial mobile communication networks, forming a seamless three-dimensional global coverage and achieving the development goal of broadband mobile communication without blind spots [2]. Communication with giant constellations of LEO satellites will be one of the new frontiers of connectivity leading to 6G, complementing terrestrial networks and providing unlimited connectivity anywhere, thus helping to bridge the digital divide [3].

Most of the current LEO satellites use L or UHF bands, which are already very crowded at present, and the fixed spectrum allocation method makes a large portion of the designated spectrum used occasionally, which leads to low spectrum utilization [4]. Therefore, spectrum sensing techniques need to be accessed to deal with the problem of spectrum inefficiency. Spectrum sensing can find available spectrum resources in both space-time dimensions and effectively improve spectrum utilization efficiency. Spectrum sensing algorithms have been extensively studied by scholars and will be reviewed in detail in Section 2. Aiming at the problems of the poor real-time performance of spectrum sensing algorithms for LEO satellite networks, poor performance at low signal-to-noise ratio (SNR), and traditional spectrum sensing algorithms can only detect signals one by one, this paper proposes an ANN-based intelligent spectrum sensing algorithm for space-based satellite networks, which can have high detection accuracy with low time delay and low energy consumption, and effectively improve spectrum utilization efficiency. The main contributions of this paper are as follows.

1) Combining the energy detection method with artificial intelligence, replacing the threshold comparison part of the traditional energy detection method with an ANN module, and proposing an ANN-based energy detection method, which solves the problem of difficult threshold setting of traditional energy detection method and has high detection probability even in low SNR environment.
2) GEO satellites are introduced based on LEO satellites, and their strong arithmetic power and storage capacity can be used to make fast and effective judgments on the spectrum status of LEO satellites.
3) Using the wide area of satellite coverage, the algorithm can sense multiple spectrums at the same time, effectively improving the efficiency of spectrum sensing.

This paper is organized as follows. Section 2 presents related work, and in Section 3, a hybrid GEO/LEO double-layer satellite constellation and information fusion algorithm for GEO satellites are designed based on the Walker constellation. In Section 4, we derive the formula that any two satellites in a space-based network can establish an inter-satellite link. Then, our proposed ANN-based energy detection method for inter-satellite spectrum state sensing is presented in detail, and finally, the sensing quality is evaluated in terms of sensing delay and sensing energy consumption. In Section 5, simulations are conducted using MATLAB software, and the results show that the ANN-based energy detection method

outperforms the conventional energy detection method. Conclusions are drawn in Section 6.

2. Related Work

With the continuous development of satellite network technology, the number of satellites is increasing, especially LEO satellites, with lower orbital altitude, the coverage of satellites for the ground is constantly changing, and GEO and LEO satellites have their characteristics in terms of coverage, service quality, and system construction and deployment, etc. Many typical communication and navigation satellite systems use a mixed constellation structure of GEO and LEO to achieve global services and provide Many typical communication and navigation satellite systems have adopted a hybrid constellation structure for global services, providing differentiated and personalized service capabilities [5]. The hybrid GEO and LEO satellites constellation network can combine the advantages of different orbits, with flexible networking, especially when the LEO satellite mission is busy, GEO can relieve the pressure of LEO node blockage. Yan et al. [6] developed conditions for establishing inter-layer links for IGSO/MEO two-layer satellite networks, taking into account beam coverage. Ge et al. [7] proposed a heterogeneous framework combining GEO and LEO systems with a NOMA scheme to multiplex frequency resources and improve spectral efficiency, taking into account the uplink. Tengyue et al. [8] use the backbone/access network model and the "moderately connected" interstellar link concept to design a dual LEO/MEO link layer network architecture that meets the quality of service while reducing the complexity of the network system. Ge et al. [9] established a GEO/LEO dual-layer satellite network architecture in a frequency coexistence scenario, taking into account the channel and dynamic characteristics between satellite nodes, and improving the spectral efficiency and signal reception reliability of GEO satellites.

For satellite spectrum sensing algorithms, Hu et al. [10] combined distributed cooperative sensing network with cognitive satellite ground network and proposed an EE formulation for cognitive network based on distributed cooperative sensing results to improve the sensing performance. Wang et al. [11] used DSC system to improve the sensing performance of weak signals and proposed a new cooperative spectrum sensing method with high detection probability even when the signal is relatively weak. Zheng. [12] used the gamma approximation to derive the false alarm probability and improve the detection probability of energy detection, and then introduced a closed expression for the AUC value under Gaussian channel to improve the traditional energy detection method.

Conventional spectrum sensing mostly requires setting thresholds, which require a priori knowledge of the noise distribution or the received signal [13], is highly susceptible to SNR, and has certain limitations in detection results [14]. Based on the traditional algorithm, combining the popular machine learning and deep learning techniques [15], it can greatly improve the spectrum detection probability. Wu et al. [16] proposed an energy detection method based on short sliding windows for detecting the presence of burst signals in a short period. Simulation results show that the missing detection probability of this method is lower than the conventional detection probability in the presence of burst signals. Nandakumar et al. [17] proposed an intelligent energy detection method based on the gamma distribution and central limit theory to derive an average detection probability formula, which improves the detection performance. Zheng et al. [18] derived a new detection probability and false alarm probability based on central limit theory and then analyzed the detection performance of the CSS the detection performance of the system is analyzed and the traditional energy detection method is optimized. Krishnakumar et al. [19] introduced decision tree classification and random forest classification from machine learning (ML) to the cyclic steady state method and

energy detection method, which has high detection probability even at low signal-to-noise ratio, and the method achieves intelligent spectrum sensing with the help of ML classification technique.

All these methods can achieve good performance in satellite communication application scenarios, but all of them invariably require a large amount of sampled data and a large amount of parallel computation. In order to reduce the complexity of the algorithm while ensuring the detection probability, an ANN-based energy detection method is proposed, which combines the robustness of neural networks and the simplicity of traditional energy detection algorithms, while introducing GEO satellites to obtain the visual relationship between LEO satellites and GEO satellites through interplanetary situational sensing, and the sensing satellites in the LEO layer upload the sensing information through the interplanetary link to the GEO satellite through the interplanetary link, uses its strong arithmetic power and storage, and then uses the GEO satellite to apply the algorithm to make fast and effective judgments on the spectral state of the LEO layer, and the algorithm also has good performance at low SNR.

3. Satellite constellation model

3.1 Double-layer satellite constellation

This paper designs a hybrid GEO/LEO double-layer satellite constellation based on the Walker constellation, first proposed by Walker J G [20], which is special in that it has the following characteristics: the constellation orbits are inclined circular orbits; the constellation has a high degree of symmetry, with all satellites orbiting at the same altitude and inclination, and with the same angle between orbital planes All satellites have the same altitude and inclination, and the same angle between orbital planes. Therefore, the geometrical characteristics of any one satellite in the constellation can replace those of the others.

The parameter $Q/P/F$ is generally used to represent the satellite orbits of the Walker constellation. Where Q denotes the number of satellites in the constellation, P denotes the number of orbital planes in the constellation and F denotes the phase factor of the constellation [21]. In the Walker constellation, assuming that a is the number of a particular satellite, the ascending node equinox V_a and the ascending node angular distance ϕ_a of that satellite are expressed as (1):

$$\begin{cases} V_a = 360\frac{P_a-1}{P} \quad (P_a = 1,2,\cdots,P) \\ \phi_a = 360\frac{P}{U}(Q_a-1) + 360\frac{F}{Q}(P_a-1) \quad (Q_a = 1,2,\cdots,U-1) \end{cases} \tag{1}$$

where U denotes the total number of satellites in each orbital plane in the Walker constellation, P_a denotes the number of satellites in orbit, and Q_a denotes the number of the orbit in which satellite a is located.

The LEO layer satellites were selected from the Walker constellation in the configuration $64/8/1$, with an orbital altitude of 800 KM and an orbital inclination set at 60°, with 64 LEO satellites evenly distributed over 8 orbital planes. The purpose of adding three GEO satellites to the LEO layer satellites is to fuse the information sensed by the LEO satellites with the GEO satellites to give a spectrum decision, and three GEOs will enable coverage of all LEO satellites. **Fig. 1** shows the GEO/LEO double-layer satellite network topology.

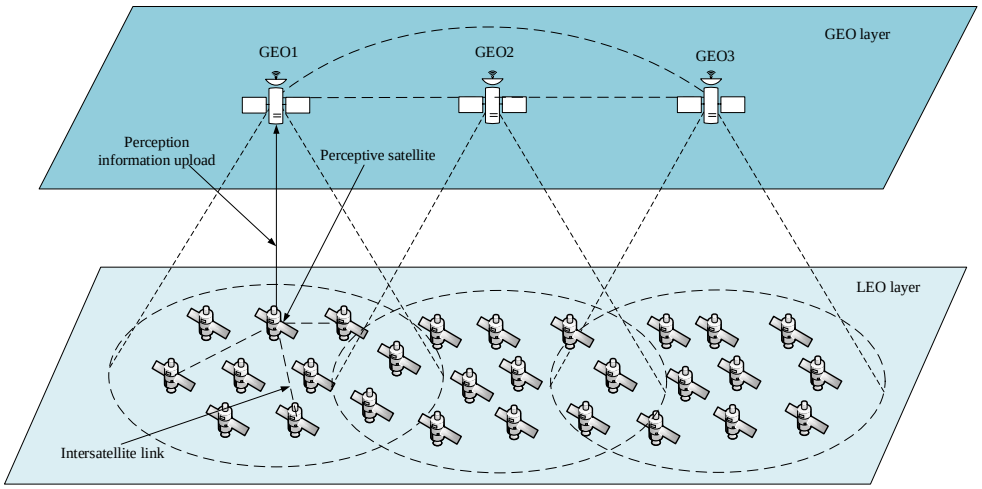

Fig. 1. GEO/LEO satellite network topology

3.2 Information fusion algorithm

In this paper, a soft judgment fusion algorithm is used. After the LEO sensing satellite has completed the local sensing data acquisition, it does not give a judgment result but uploads the collected raw data to the GEO information fusion center. Therefore, even if a small error occurs during the transmission process, it will not affect the final verdict. This fusion method increases the complexity of the algorithm but improves the detection probability. The data transmission process is shown in **Fig. 2**.

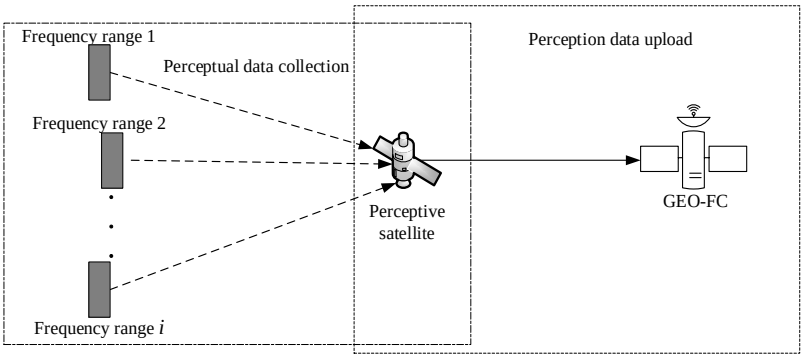

Fig. 2. Schematic of GEO soft judgment

4. Intelligent spectrum sensing

The interplanetary spectrum sensing algorithm should keep the detection probability while keeping the sensing delay and energy consumption as low as possible. The algorithm in this paper consists of three parts: the interplanetary link situational sensing phase, the interplanetary spectrum state sensing phase, and the sensing quality assessment phase.

4.1 Interstellar link situational sensing

Visibility between two satellites is a prerequisite for establishing a link for inter-satellite spectrum sensing. In general, two conditions are generally met for satellite visibility: geometric visibility and antenna visibility.

4.1.1 Geometric visual conditions

Assuming that R_e denotes the radius of the Earth, as shown below, the communication links of satellite S_A and satellite S_B are tangent to the atmosphere at that moment.

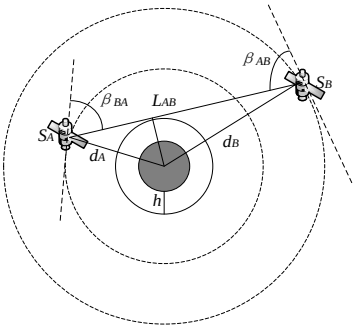

Fig. 3. Satellite geometry view

From **Fig. 3**, satellite S_A and satellite S_B establish an inter-satellite link as in (2).

$$\begin{cases} \theta_A > -\beta_{BA} \quad or \quad \theta_B > -\beta_{AB} \\ \beta_{AB} = \arccos\left[\frac{R_e+h}{R_e+d_A}\right] \\ \beta_{BA} = \arccos\left[\frac{R_e+h}{R_e+d_B}\right] \end{cases} \tag{2}$$

where θ_A denotes the pitch angle of satellite S_B relative to satellite S_A and θ_B denotes the pitch angle of satellite S_A relative to satellite S_B. Translating the above equation into a distance is expressed as (3).

$$L_{AB} < \sqrt{(R_e + d_A)^2 - (R_e + h)^2} + \sqrt{(R_e + d_B)^2 - (R_e + h)^2} \tag{3}$$

4.1.2 Antenna visibility conditions

An inter-satellite link can only be established between satellites if both satellites are in the scanning range of both antennas, as shown in **Fig. 4**.

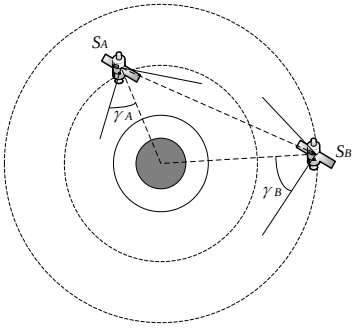

Fig. 4. View of the satellite dish

For satellites S_A and S_B to satisfy the chain building condition, they should also satisfy the relationship in (4).

$$\theta_A > \gamma_A - 90^\circ \quad or \quad \theta_B > \gamma_B - 90^\circ \tag{4}$$

Translate the above equation into a distance representation as (5).

$$L_{AB} > （R_e + d_A） cos\gamma_A + (R_e + d_B) cos\gamma_B \tag{5}$$

In summary, the conditions for the establishment of an inter-satellite link between the two satellites are as follows:

$$(R_e + d_A) cos\gamma_A + (R_e + d_B) cos\gamma_B < L_{AB} < \sqrt{(R_e + d_A)^2 - (R_e + h)^2} + \sqrt{(R_e + d_B)^2 - (R_e + h)^2} \tag{6}$$

4.2 Inter-satellite spectrum state sensing

In the interplanetary spectrum state sensing phase, the transmission loss of the signal in the channel is first objectively analyzed and then the received signal is detected using ANN-based energy detection to determine the occupation status of the band.

4.2.1 Path cost of signal transmission

Based on the wide area of satellite coverage, it is assumed that the sensing satellite can receive signals in M frequency bands, with M signals denoted as $x = [x_1, x_2, \cdots, x_M]^T$. When the signals are transmitted in the channel, they will be interfered by Doppler shift, path fading ,and noise, affecting the signal quality at the receiving end. **Fig. 5** shows the inter-satellite channel transmission model, assuming M Gaussian noise signals as $n = [n_1, n_2, \cdots, n_M]^T$.

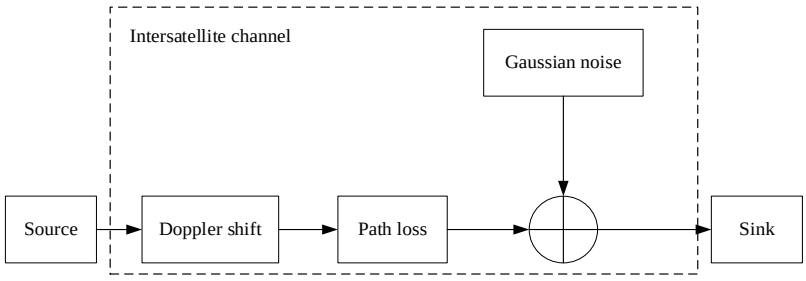

Fig. 5. Inter satellite channel model diagram

The resulting Doppler shift is given by (7).

$$f_d = f \cdot \frac{|\boldsymbol{v}|}{c} \cdot \frac{\boldsymbol{R} \cdot \boldsymbol{v}}{|\boldsymbol{R}| \cdot |\boldsymbol{v}|} = f \cdot \frac{\boldsymbol{R} \cdot \boldsymbol{v}}{c \cdot |\boldsymbol{R}|} \tag{7}$$

where f is the carrier frequency (Hz) transmitted by the satellite, c is the speed of light in a vacuum ($m \cdot s^{-1}$), $\boldsymbol{R}$ is the distance vector and $\boldsymbol{v}$ is the velocity vector.

When the unit of d is km and the unit of f is GHz, the free space propagation loss ξ is given by (8).

$$\xi = \frac{\lambda^2}{(4\pi)^2 d^2} = \frac{c^2}{(4\pi d f)^2} \tag{8}$$

Then the signal received by the sensing satellite is $y = [y_1, y_2, \cdots, y_M]^T$ and the frequency is $f + f_d$.

$$y_i = \xi * x_i + n_i \ , i = 1,2, \cdots, M \tag{9}$$

4.2.2 ANN-based multi-node inter-satellite spectrum sensing algorithm

Spectrum sensing is the detection of the presence of a signal $x(t)$ in a frequency band, a problem that can be translated into a binary hypothesis test, with H_0 indicating that only noise is present, i.e., the spectrum is free, and H_1 indicating that a signal is present, i.e., the spectrum is occupied.

$$y(t) = \begin{cases} n(t) & : H_0 \\ \xi * x(t) + n(t) & : H_1 \end{cases} \quad 0 < \xi < 1 \tag{10}$$

The most common and simplest method of spectrum sensing is energy detection [22] (Energy Detection, ED), which is a non-coherent detection process. As shown in **Fig. 6**, in the energy detection method, after the signal $y(t)$ is received, N denotes the number of signal sampling points, and the cumulative energy at N points of this signal is calculated and then compared with the threshold value λ indicating the noise energy, thus completing the detection of the signal. The traditional energy detection method does not use a priori knowledge of the signal and is not complicated to implement, but it is difficult to set a suitable threshold, especially at low SNR, where noise will annihilate the less energetic signal, making the performance of the energy detection method fall off a cliff.

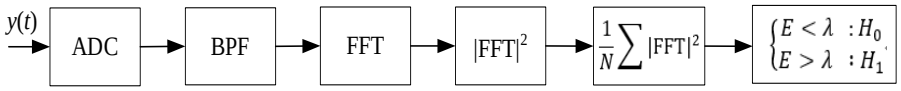

Fig. 6. Flow chart of energy detection method

The fixed spectrum allocation method makes a large portion of the designated spectrum used occasionally, resulting in low spectrum utilization. Therefore, intelligent spectrum sensing technology is needed to deal with the problem of low spectrum efficiency. Intelligent spectrum sensing can find available spectrum resources in both space and time dimensions, effectively improving spectrum utilization efficiency. The combination of the energy detection method with support vector machines (SVM) in Saber et al. [23] is well validated in Bicaïs et al. [24]. This paper combines the energy detection method with a neural network and proposes an ANN-based energy detection method (ANN-ED), as shown in **Fig. 7**. The algorithm replaces the energy and threshold comparison part with an ANN module, to improve the detection probability at low signal-to-noise ratios.

Assuming that the number of samples of the received signal through the BPF is N', the $|\mathrm{FFT}|^2$ of these samples is used as input to the neural network, which is used to automatically adjust the weight of each $|\mathrm{FFT}|^2$ and then give an objective spectral decision. The algorithm makes full use of the simplicity of the energy detection method and the robustness of the neural network to find the characteristics of the received signal with and without $x(t)$ by means of the neural network, solving the problems of the traditional energy detection method in terms of difficulty in setting thresholds and deteriorating performance at low signal-to-noise ratios.

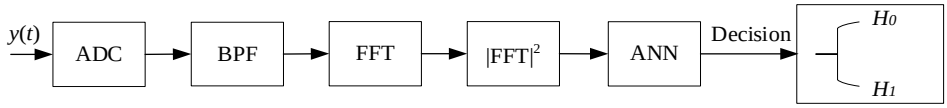

Fig. 7. ANN-based energy detection flow chart

Most traditional energy detection methods are based on single signal-by-signal detection. Using the wide area of sensing satellite coverage, signals from several different frequency bands are received simultaneously, and the occupancy status of multiple frequency bands can be detected simultaneously. The ANN-based multi-node energy detection method is shown in **Fig. 8**.

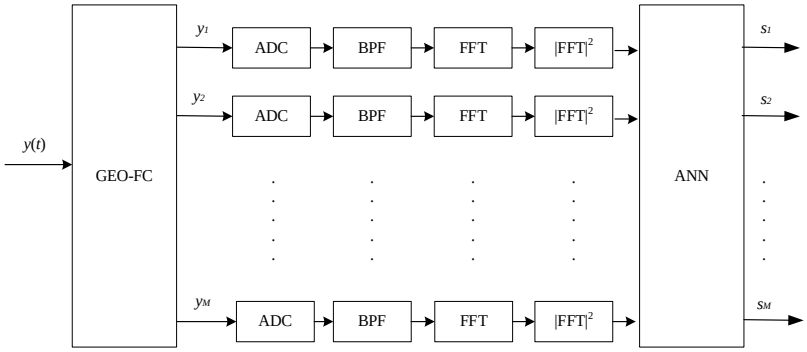

Fig. 8. ANN-based multi-node energy detection flow chart

In the GEO information fusion center, the signals are weighted and fused when receiving signals from different frequency bands sent by sensing satellites. The magnitude of the received SNR determines the assignment of the weighting coefficients [25], which are calculated as (11).

$$\beta_i = \frac{\gamma_i}{\sqrt{\sum_{i=1}^{M} \gamma_i}} \tag{11}$$

where γ_i denotes the SNR of the ith signal received, $i = 1,2,\cdots,M$.

The quantized received signal is $Y = [\beta_1 Y_1, \beta_2 Y_2, \cdots, \beta_M Y_M]^T$, where $Y_i = [y_{i1}, y_{i2}, \cdots, y_{iN}]$, $i = 1,2,\cdots,M$. Assuming that the satellite's BPF bandwidth is Fs and the spectrum sensing period is T, according to Nyquist's sampling theorem, the satellite's sampling frequency is $2Fs$ when the information of the original signal can be preserved intact. The filtered signal is then subjected to an FFT, noted as $Y(f) = [Y_1(f), Y_2(f), \cdots, Y_M(f)]^T$, where $Y_i(f) = [Y_{i1}(f), Y_{i2}(f), \cdots, Y_{iN'}(f)]$, $i = 1,2,\cdots,M$.

The input to the ANN is then expressed as (12).

$$x_{M\times N'} = Y(f) = \begin{bmatrix} |Y_{11}(f)|^2 & |Y_{12}(f)|^2 & \cdots & |Y_{1N'}(f)|^2 \\ |Y_{21}(f)|^2 & |Y_{22}(f)|^2 & & |Y_{2N'}(f)|^2 \\ \vdots & & \ddots & \vdots \\ |Y_{M1}(f)|^2 & |Y_{M2}(f)|^2 & \cdots & |Y_{MN'}(f)|^2 \end{bmatrix} \tag{12}$$

The ANN internal formula is given by (13).

$$b_{l\times M}=\begin{bmatrix}\omega_{11} & \omega_{12} & \cdots & \omega_{1N'}\\ \omega_{21} & \omega_{22} & & \omega_{2N'}\\ \vdots & & \ddots & \vdots\\ \omega_{l1} & \omega_{l1} & \cdots & \omega_{lN'}\end{bmatrix}[x_{M\times N'}]^T+\begin{bmatrix}u_{11} & u_{12} & \cdots & u_{1M}\\ u_{21} & u_{22} & & u_{2M}\\ \vdots & & \ddots & \vdots\\ u_{l1} & u_{l1} & \cdots & u_{lM}\end{bmatrix} \tag{13}$$

where each row of the input matrix $x_{M\times N'}$ corresponds to the $|\mathrm{FFT}|^2$ of one received signal sampling point, the matrix $\omega_{l\times N'}$ represents the weight matrix, each element corresponds to the weight of each input point, and l represents the number of hidden layer neurons. each column of $b_{l\times M}$ corresponds to the computed result of one received signal.

In this paper, the sigmoid function is chosen as the activation function. This function is non-linear and can approximate any function.

$$f(x)=\frac{1}{1+e^{-x}} \tag{14}$$

Then the output of ANN is given by (15).

$$s=f(b_{lM})=[s_1 \quad s_2 \quad \cdots \quad s_M] \tag{15}$$

where,

$$s_i=\begin{cases}1, & s_i^s>\zeta\\ 0, & other\end{cases} \tag{16}$$

s_i^s denotes the output of the sigmoid activation function, if s_i =0, it means the detected band is spare, if s_i =1, it means the detected band is occupied, ζ denotes the decision threshold. $i=1,2,\cdots,M$.

4.3 Sensing quality assessment

The quality of the sensing is assessed by two indicators, namely the spectrum sensing latency and the energy consumption. In the process of spectrum sensing, it is important to keep the sensing latency as low as possible and the energy consumption as low as possible, while ensuring the probability of detection.

The nodal delay within the star is assumed to be $T_L(g,i)$, which is the signal processing delay after signal i is received by sensing satellite g; g denotes the sensing satellite that received the frequency request, i denotes the signal received in band i, where $g=1,2,\cdots,64$ and $i=1,2,\cdots,M$.

$$T_L(g,i)=N\cdot\frac{1}{Fs_{BPF}(g,i)}+t \tag{17}$$

where $Fs_{BPF}(g,i)$ denotes the sampling frequency of the signal in the ith band received by sensing satellite g, and t denotes the system time delay during the in-satellite judgment of the spectrum state.

Assuming that E denotes the perceived energy consumption of a sensing session, combined with the perceived time delay, the objective function and constraints are given by (18).

$$\begin{gathered} min\{E\} = min\{E_{LEOgi} + E_i\} \\ s.t. \forall g = 1,2,\cdots,64, \quad \forall i = 1,2,\cdots,M \\ E_{LEOgi} = P_{LEOgi} T_L(g,i) \\ E_i = N \cdot b_s \cdot E_e \\ T_L(g,i) \leq T_{max} \end{gathered} \tag{18}$$

where P_{LEOgi} denotes the power of the ith signal received by sensing satellite g, E_i denotes the energy consumption of the GEO satellite to adjudicate the ith band state, E_e denotes the energy consumption at the receiving end, and T_{max} denotes the maximum time delay within sensing satellite g during spectrum sensing.

5. Simulation results and analyses

5.1 Inter-satellite Spectrum Sensing Scenarios

In this paper, we use STK to create a GEO/LEO double-layer satellite network, naming the 64 LEO satellites as LEO_g, $g = 1,2,\cdots,64$. 3 GEO are named GEO_c, $c = 1,2,3$. 3 GEOs evenly distributed in GEO. LEO1 is selected as the sensing satellite and the sensing time is 0:00 am on April 17, 2022, denoted as t_0. LEO operates at a period of approximately 80 min, with 8 satellites in each orbit, so the sensing period is set to 10 min and the visibility matrix is updated every 10 min.

The sensing satellite receives signals from several different frequency bands and then uploads the raw data to the GEO Information Fusion Centre, which adjudicates the spectral state of the LEO layer through its powerful computing and storage capabilities. Simulations using Satellite Tool Kit software yielded 2D and 3D plots of the Walker constellation, as shown in **Fig. 9**.

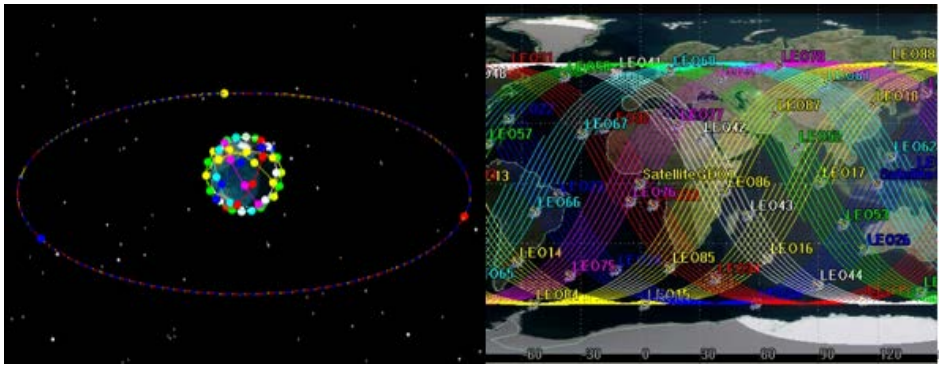

Fig. 9. GEO/LEO double layer constellation constructed by STK

5.2 Simulation of real spectrum environment

This paper simulates the interplanetary channel scenario using a white Gaussian channel with a sensing spectrum of 300 MHz-800 MHz and a bandwidth of 500 MHz, setting the bandwidth of a single band at 10 MHz, which can be divided into a total of 50 bands. In order to simulate the real satellite spectrum environment, the signal needs to be simulated. In this paper, the

inter-satellite service signal (FM signal) is generated based on the ON/OFF source model, assuming that the signal arrival process obeys Poisson distribution with parameter λ, the average interval time of signal arrival obeys exponential distribution with parameter μ, and the signal duration obeys geometric distribution with parameter ε. The model parameters are set as shown in **Table 1**.

Table 1. Model parameter settings

Model parameter	Parameter value
λ	0.2
μ	5
ε	0.2
T_{max}/ms	2
E_e/nJ	50
$b_s/bit \cdot s^{-1}$	1

All 64 LEO satellites and 3 GEO satellites are taken, and the visibility relationship between satellites is analyzed by STK to get the satellite's chain building at any moment, then the satellite's visibility matrix is imported into MATLAB through the interface, and the satellite's channel (300 MHz-800 MHz) is modeled by MATLAB to simulate the path loss and Doppler shift between satellites.

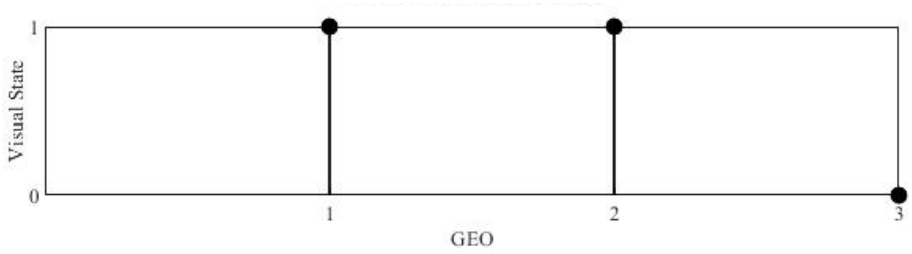

Fig. 10. Visual relationship diagram of LEO1 and GEO

Fig. 10 shows the visual relationship between LEO1 and GEO satellites at that moment. The visual relationship between the sensing satellite LEO1 and GEO satellites is obtained by interplanetary situational awareness, where 1 indicates that the two satellites are visible and an interplanetary link can be established, and 0 indicates that the two satellites are not visible. From the **Fig. 10**, we know that LEO1 is visible with GEO1 and GEO2, and LEO1 will establish an interplanetary link with GEO1.

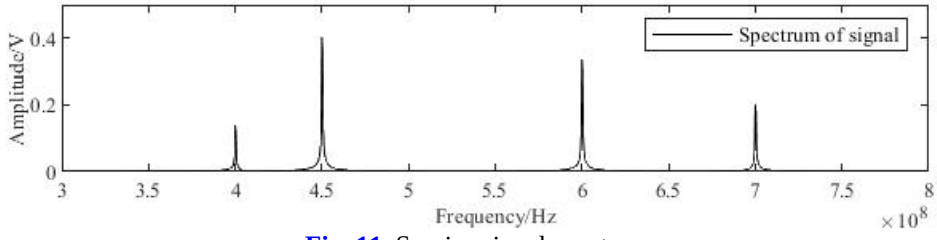

Fig. 11. Service signal spectrum

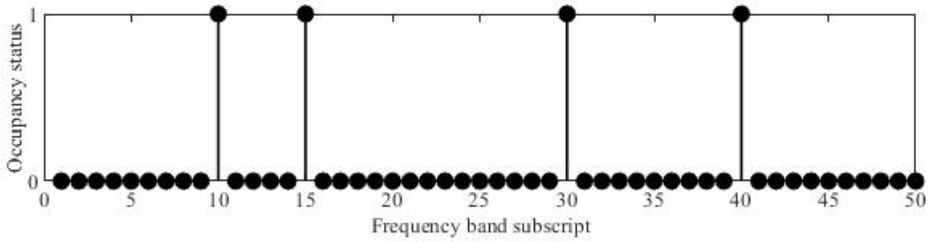

Fig. 12. Occupancy status chart for each frequency band

At the moment t_0, the spectrum of the service signal generated by the source model is shown in **Fig. 11**. The signal is then analyzed for spectrum occupancy, and **Fig. 12** shows the occupancy of the signal from 300 MHz to 800 MHz, with 1 indicating that the band is in the occupied state and 0 indicating that the band is in the spare state. At the moment t_0, bands 10, 15, 30 and 40 are occupied and the rest of the bands are spare.

5.3 Performance evaluation of the ANN-ED algorithm

In this paper, the ANN module contains an input layer, a hidden layer and an output layer with a total of three topologies. In the actual satellite spectrum environment, the SNR is not constant, so signals with different SNRs are required for training the network to improve the detection performance of the network. MATLAB is used to generate a signal database that consists of FM signals with different SNRs (SNR∈[-25dB, -5dB]) of FM signals and Gaussian white noise signals, where the FM signal corresponds to an output of 1 and only the Gaussian white noise corresponds to an output of 0. The number of sampling points N of the signals is 4096. To ensure that the number of signals meets the test requirements, we compare the detection probabilities P_d of different numbers of signals (l=20), as shown in **Table 2**.

Table 2. Detection probability for different numbers of signals

	Signal Type	Training	Test	P_d
1	Signal and Noise	1400	700	0.9871
	Noise	200	200	
2	Signal and Noise	2800	1400	0.9829
	Noise	400	400	
3	Signal and Noise	3500	2100	0.9857
	Noise	800	800	

The detection performance of the network with SNR∈[-25dB, -5dB] is shown in **Table 2**. By comparing the detection probabilities of different numbers of training and test sets, it is clear that the detection probability of class 1 is the highest. Then we divide the training set and test set for class 1 data. And the detection probability of the network at different division ratios is shown in **Table 3**.

Table 3. Detection probabilities for different division ratios

Signal Type	Training	Test	proportion	P_d
Signal and Noise	1200	900	3:2	0.9171
Noise	300	100		
Signal and Noise	1400	700	16:9	0.9871
Noise	200	200		
Signal and Noise	1500	600	7:3	0.9314
Noise	250	150		

From **Table 3**, it can be seen that the network with the division ratio of 16:9 has the best detection performance and the best performance of the neural network, which can guarantee the correctness of the test results. Combining the results in **Table 2** and **Table 3**, within SNR∈[-25dB, -5dB], taking a step size of 1, each SNR corresponds to 100 FM signals, for a total of 2100 FM signals, and then 400 Gaussian white noise signals are generated, and the signal database is composed of these 2500 signals. Each FM signal corresponds to a label of 1, and each noise signal corresponds to a label of 0. After disordering the 2100 FM signals, the training and test sets are divided in the ratio shown in **Table 4**.

Table 4. Division of data sets

Signal Type	Training	Test
Signal and Noise	1400	700
Noise	200	200

The overall detection performance of the network at SNR∈[-25dB, -5dB] can be obtained by training the network with the ratios divided in **Table 4**.

To determine the number of neurons in the hidden layer, this paper uses a more intuitive approach by testing the spectral detection probability P_d and the false alarm probability P_f of the system under different numbers of neurons. **Table 5** shows the detection performance of the system with different numbers of neurons.

Table 5. Detection performance of a different number of neurons

l	P_d	P_f
5	0.9829	0.0138
10	0.9771	0.0288
20	0.9857	0.0138
40	0.9929	0.0075
60	0.9814	0.0163
80	0.9843	0.0088

It can be seen that the system has the best detection probability of 0.9929 and false alarm probability of 0.0075 when the number of neurons is 40 and the SNR∈[-25dB, -5dB].

After training the neural network, the spectral environment with different SNRs in Section 5.2 is then simulated. The sensing satellite LEO1 uploads the received signals of different frequency bands to the GEO1 information fusion center, and GEO1 weights the signals of different frequency bands by SNR, and then applies these two methods to judge the occupancy

status of each band separately. A comparison of the detection performance of the ANN-ED method with the traditional energy detection method for SNR∈[-25dB, -5dB] is given in **Fig. 13**. Where the number of Monte Carlo experiments for each SNR case is set to 1000.

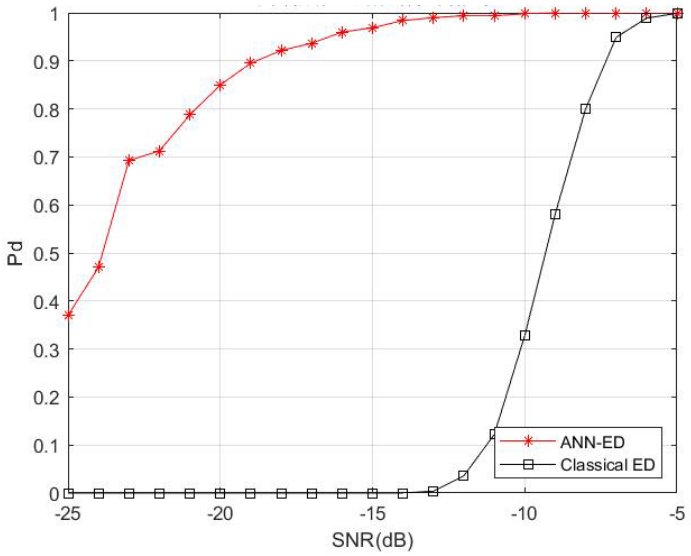

Fig. 13. Probability diagram for spectral detection by different methods

Fig. 13 shows the comparison of the detection probability of different spectrum detection methods at different SNRs. The performance of the traditional energy detection method drops precipitously at low SNRs, with a probability of only about 10% at a SNR of -11 dB. The detection probability of ANN-ED method at low SNR is greatly improved, reaching 90% detection probability at SNR of -19 dB. The detection probability reaches 100% at a SNR of -10 dB. This is because it is very difficult to set the threshold value in the conventional energy detection method. When the SNR deteriorates, a noisy signal with very high interference is recognized as a useful signal, and therefore a weak signal with low energy cannot be recognized.

The performance improvement of the algorithm proposed in this paper has the following reasons. First, the proposed algorithm trains the ANN with the signal and noise at each SNR and the corresponding spectral state, and through continuous optimization, automatically finds the relationship between signal and noise at different SNRs, with a high probability of detection even when the SNR deteriorates. Secondly, the AI algorithm is introduced into the traditional energy detection method, which combines the simplicity of energy detection method and the robustness of neural network, and is able to detect the occupation status of multiple frequency bands at the same time, effectively improving the efficiency of spectrum detection. Finally, the proposed algorithm only needs to sample N' points in the signal that can pass through the filter passband, which reduces both the latency and energy consumption of the system, thus reducing the overhead of spectrum sensing for the entire satellite network.

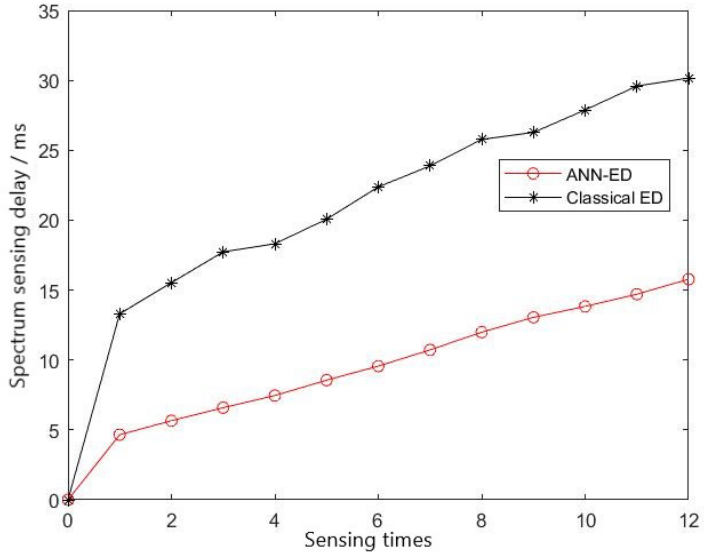

Fig. 14. Relationship between sensing delay and sensing number of times

The relationship between the sensing delay and the number of sensing times is shown in **Fig. 14**. As the number of spectrum sensing times increases, the sensing delay of the traditional energy detection method and the ANN-ED method gradually increases, and the delay of the ANN-ED method is much smaller than that of the traditional energy detection method, because the traditional energy detection method has to detect each signal one by one, while the ANN-ED method can detect signals of multiple frequency bands at the same time, which makes the spectrum sensing delay significantly reduced.

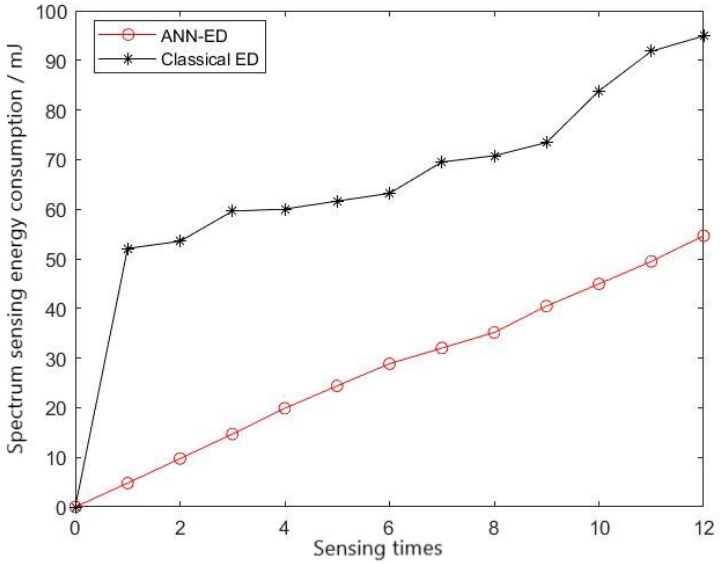

Fig. 15. Relationship between sensing energy consumption and sensing number of times

The energy consumption of sensing versus the number of sensing times is shown in **Fig. 15**. For the ANN-ED method, when the transmission rate is 1 $bit \cdot s^{-1}$ and the number of sensing times is 12, the sensing energy consumption is approximately 53.7 mJ, which is much

lower than that of the traditional energy detection method. Because the traditional energy detection method requires all nodes sampled in the system to participate in the energy detection at each detection, while the ANN-ED method only requires some of the nodes N', the system sensing can make the energy consumption much smaller than the traditional energy detection method even though the delay is guaranteed to be low.

6. Conclusion

In this paper, an ANN-based intelligent spectrum sensing algorithm for space-based satellite networks is proposed to make fast and effective judgments on the spectrum status of LEO satellites with the help of the strong computing power of GEO satellites. A two-layer satellite network consisting of 3 GEO satellites and 64 LEO satellites is constructed. In the inter-satellite link situational sensing phase, the visibility relationship between satellites is analyzed to obtain the visibility matrix between satellites at the current moment and set the detection period to periodically update the visibility matrix between satellites. In the inter-satellite spectrum state sensing phase, the sensing satellite LEO uploads the sensing information to the GEO information fusion center, and then the GEO applies the trained ANN-ED algorithm to make objective judgments on the received signals and give spectrum decisions. In the sensing quality assessment phase, the sensing delay and sensing energy consumption are analyzed. The simulation results show that the ANN-based energy detection method has a higher detection probability and less delay and energy consumption for spectrum sensing than the traditional energy detection method. Finally, the topological changes of the satellite network are detected periodically and the visual matrix of the satellite is corrected in real time.

In future research, we will consider how to further improve the spectrum detection probability and reduce the spectrum sensing delay based on the research work in this paper, and implement the spectrum allocation based on the spectrum sensing algorithm proposed in this paper.

References

[1] L. Wang, Q. Wang, L. Jin, J. Zhu, P. Chen, and J. Han, "Research and Application Exploration of 6G Communication Network System Architecture," in *Proc. of 2022 IEEE 2nd International Conference on Electronic Technology, Communication and Information (ICETCI)*, Changchun, China, pp. 742-745, 2022. Article (CrossRef Link).

[2] S. Chen, Y. -C. Liang, S. Sun, S. Kang, W. Cheng, and M. Peng, "Vision, Requirements, and Technology Trend of 6G: How to Tackle the Challenges of System Coverage, Capacity, User Data-Rate, and Movement Speed," *IEEE Wireless Communications*, Vol. 27, No. 2, pp. 218-228, Apr. 2020. Article (CrossRef Link).

[3] M. Giordani and M. Zorzi, "Non-Terrestrial Networks in the 6G Era: Challenges and Opportunities," *IEEE Network*, Vol. 35, No. 2, pp. 244-251, Mar./Apr. 2021. Article (CrossRef Link).

[4] W. Sun, X. Liu, K. Zheng, Y. Xu, and J. Liu, "Spectrum Utilization Improvement for Multi-Channel Cognitive Radio Networks with Energy Harvesting," in *Proc. of 2021 International Conference on Networking and Network Applications (NaNA)*, Lijiang City, China, pp. 1-7, 2021. Article (CrossRef Link).

[5] Z. Lu, J.Z. Tian, J. Zhao, and W.C. Zhao, "Design of management and control architecture for high-low orbit hybrid satellite network," *Journal of China Academy of Electronic Science*, Vol. 15, No. 1, pp. 15-19, 2020. Article (CrossRef Link).

[6] H. Yan, Y. Zhang, R. Zhang, L. Zeng, and W. Jia, "Inter-layer Topology Design for IGSO/MEO Double-Layered Satellite Network with the Consideration of Beam Coverage," in *Proc. of 2018 IEEE 18th International Conference on Communication Technology (ICCT)*, Chongqing, China, pp.750-754, 2018. Article (CrossRef Link).
[7] R. Ge, D. Bian, J. Cheng, K. An, J. Hu, and G. Li, "Joint User Pairing and Power Allocation for NOMA-Based GEO and LEO Satellite Network," *IEEE Access*, Vol. 9, pp. 93255-93266, 2021. Article (CrossRef Link).
[8] M. Tengyue, Y. Weibing, and Z. Jingjing, "Design of LEO/MEO Double-Layer Satellite Network," in *Proc. of 2019 6th International Conference on Information Science and Control Engineering (ICISCE)*, Shanghai, China, pp. 1022-1026, 2019. Article (CrossRef Link).
[9] R. Ge, D. Bian, K. An, J. Cheng, and H. Zhu, "Performance Analysis of Cooperative Nonorthogonal Multiple Access Scheme in Two-Layer GEO/LEO Satellite Network," *IEEE Systems Journal*, Vol. 16, No. 2, pp. 2300-2310, Jun. 2022. Article (CrossRef Link).
[10] J. Hu, G. Li, D. Bian, S. Shi, R. Ge, and L. Gou, "Energy-Efficient Cooperative Spectrum Sensing in Cognitive Satellite Terrestrial Networks," *IEEE Access*, Vol. 8, pp. 161396-161405, 2020. Article (CrossRef Link).
[11] Y. Wang, X. Ding, J. Li, T. Hong, and G. Zhang, "Performance analysis of Spectrum Sensing based on Distributed Satellite Clusters," in *Proc. of 2022 IEEE/CIC International Conference on Communications in China (ICCC Workshops)*, Sanshui, Foshan, China, pp. 65-70, 2022. Article (CrossRef Link).
[12] Y. Zheng, "Performance of Improved Energy Detection in Gaussian Channel," in *Proc. of 2021 IEEE International Conference on Power, Intelligent Computing and Systems (ICPICS)*, Shenyang, China, pp. 435-438, 2021. Article (CrossRef Link).
[13] P. Nimudomsuk, M. Sanguanwattanaraks, K. Srisomboon, and W. Lee, "A Performance Comparison Of Spectrum Sensing Exploiting Machine Learning Algorithms," in *Proc. of 2021 18th International Conference on Electrical Engineering/Electronics, Computer, Telecommunications and Information Technology (ECTI-CON)*, Chiang Mai, Thailand, pp. 102-105, 2021. Article (CrossRef Link).
[14] G. Hongjian, L. Yang, A. Chunyan, and H. Biyao, "A Three-step Cooperative Spectrum Sensing Algorithm Based on Historical Sensing Information Prediction," in *Proc. of 2021 IEEE 6th International Conference on Signal and Image Processing (ICSIP)*, Nanjing, China, pp. 1198-1203, 2021. Article (CrossRef Link).
[15] Z. Shi, W. Gao, S. Zhang, J. Liu, and N. Kato, "Machine Learning-Enabled Cooperative Spectrum Sensing for Non-Orthogonal Multiple Access," *IEEE Transactions on Wireless Communications*, Vol. 19, No. 9, pp. 5692-5702, Sept. 2020. Article (CrossRef Link).
[16] W. Wu, Z. Wang, L. Yuan, F. Zhou, F. Lang, B. Wang, and Q. Wu, "IRS-Enhanced Energy Detection for Spectrum Sensing in Cognitive Radio Networks," *IEEE Wireless Communications Letters*, Vol. 10, No. 10, pp. 2254-2258, Oct. 2021. Article (CrossRef Link).
[17] S. Nandakumar, T. Velmurugan, U. Thiagarajan, and M. Karuppiah, M. M. Hassan, A. Alelaiwi and M. M. Islam, "Efficient Spectrum Management Techniques for Cognitive Radio Networks for Proximity Service," *IEEE Access*, Vol. 7, pp. 43795-43805, 2019. Article (CrossRef Link).
[18] Y. Zheng, Y. Xia, and H. Wang, "Spectrum Sensing Performance Based on Improved Energy Detector in Cognitive Radio Networks," in *Proc. of 2020 IEEE International Conference on Artificial Intelligence and Computer Applications (ICAICA)*, Dalian, China, pp. 405-408, 2020. Article (CrossRef Link).
[19] V. Krishnakumar, P. Savarinathan, T. Karuppasamy, and A. Jayapalan, "Machine Learning based Spectrum Sensing and Distribution in a Cognitive Radio Network," in *Proc. of 2022 International Conference on Computer Communication and Informatics (ICCCI)*, Coimbatore, India, pp. 1-4, 2022. Article (CrossRef Link).
[20] Y. Wei, H. Li, and X. Du, "An Efficient LEO Global Navigation Constellation Design Based on Walker Constellation," in *Proc. of 2020 IEEE Computing, Communications and IoT Applications (ComComAp)*, Beijing, China, pp. 1-6, 2020. Article (CrossRef Link).

[21] J. Y. Li, M. Hu, X. Y. Wang, F. F. Li, and J. H. Xu, "Analysis of Configuration Bias Maintenance Control Method for LEO Walker Constellation," *China's space science and technology*, Vol. 41, No. 2, pp. 38-47, 2021. Article (CrossRef Link).
[22] A. Bujunuru and T. Srinivasulu, "A Survey on Spectrum Sensing Techniques and Energy Harvesting," in *Proc.of 2018 International Conference on Recent Innovations in Electrical, Electronics & Communication Engineering*, Bhubaneswar, India, pp. 751-755, 2018. Article (CrossRef Link).
[23] M. Saber, A. El Rharras, R. Saadane, A. H. Kharraz, and A. Chehri, "An Optimized Spectrum Sensing Implementation Based on SVM, KNN and TREE Algorithms," in *Proc. of 2019 15th International Conference on Signal-Image Technology & Internet-Based Systems*, Sorrento, Italy, pp. 383-389, 2019. Article (CrossRef Link).
[24] S. Bicaïs, A. Falempin, J. -B. Doré, and V. Savin, "Design and Analysis of MIMO Systems Using Energy Detectors for Sub-THz Applications," *IEEE Transactions on Wireless Communications*, Vol. 21, No. 6, pp. 3678-3690, Jun. 2022. Article (CrossRef Link).
[25] P. Verma, "Weighted Fusion Scheme for Cooperative Spectrum Sensing," in *Proc. of 2020 International Conference on Industry 4.0 Technology (I4Tech)*, Pune, India, pp. 186-190, 2020. Article (CrossRef Link).

Xiujian Yang received a bachelor's degree. He graduated from Shandong University of Science and Technology with a bachelor's degree in communication in 2021. Master of Information and Communication Engineering, School of Computer and Communication Engineering, Beijing University of Science and Technology. His research interests include space communications, cognitive radio technologies, and resource allocation algorithms.

Lina Wang received the M.S. and Ph.D. degrees in communication and information systems from the Harbin Institute of Technology in 2001 and 2004, respectively. She is currently a Professor with the Department of Communication Engineering, School of Computer and Communication Engineering, University of Science and Technology Beijing. Her research interests include space communications, cognitive radio technologies, resource allocation algorithms, satellite positioning algorithms, and rateless codes.